Sub-seismic scale folding and thrusting within an exposed mass transport deposit: A case study from NW Argentina.

Matheus S. Sobiesiak[1], G. Ian Alsop[1], Ben Kneller[1], Juan Pablo Milana[2]

[1] Dept. of Geology and Petroleum Geology, University of Aberdeen, Aberdeen AB24 3UE, Scotland, U.K.

[2] Universidad Nacional de San Juan, Mitre Este, San Juan, Argentina

Corresponding author.

E-mail addresses: matheus.sobiesiak@gmail.com (M.S.Sobiesiak), ian.alsop@abdn.ac.uk (G.I.Alsop), b.kneller@abdn.ac.uk (B.Kneller), jpmilana@gmail.com (J.P.Milana).

Abstract

While imaging of mass transport deposits (MTDs) by seismic reflection techniques commonly reveals thrusts and large blocks that affect entire deposits, associated systems of folds are generally less apparent as they are typically below the limits of seismic resolution. However, such sub-seismic scale structures are important as they permit the direction of emplacement, gross kinematics and internal strain within MTDs to be determined. Here we present a rigorous description of two outcrop-scale MTDs exposed in La Peña gorge, northwestern Argentina. These Carboniferous MTDs enable us to illustrate structural changes from a compressional domain, marked by sets of imbricated sandstone layers, into an extensional domain, characterized by sheared blocks of sandstone embedded in a finer matrix. Folds may be progressively modified during slump translation, resulting in asymmetric folds, which undergo subsequent deformation leading to sheared fold limbs together with detached and rotated fold hinges. In order to constrain transport directions within the MTDs, we measured fold hinges, mud clast alignment, and thrust planes as kinematic indicators. We propose emplacement models for both MTDs based on the overall deformational behaviour of sandstone beds

during translation. The first model is based on the internal geometries and structures of a fault-dominated MTD, and the second model is based on layer-normal shearing in a fold-dominated MTD.

Keywords: Mass transport deposit, Kinematic indicators, Imbricate thust-faults, Layer-normal shearing, Fold deformation, Sandstone blocks

1 Introduction

Gravity-driven mass transport is an important processes in the downslope redistribution of large amounts of sediment from the continental shelf-edge and upper slope, thereby contributing to the evolution of continental margins (e.g Hampton et al. 1996; Moscardelli and Wood 2008; De Blasio et al. 2013). The deposits of these processes may locally constitute up to 80% of the stratigraphic section (Gamberi et al. 2011) and thus control deposition at the basin scale (Kneller et al. 2016). Mass transport deposits (MTDs) are highly complex and comprise the entire spectrum of deposits that formed *en masse*, via processes such as creep, slide, slump, debris flow and multiphase granular flow (e.g. Lucente and Pini 2003; Posamentier and Martinsen 2011). These are part of a continuum of processes that can evolve from one to another with time (e.g. Stow 1986; Nemec 1990; Posamentier and Martinsen 2011). Turbidity currents and their deposits are not included in the classification above; however, with time, they can evolve into debris flows (e.g. Haughton et al. 2003; Weimer and Shipp 2004), or be generated by them (e.g. Mohrig and Marr 2003; Felix and Peakall 2006). The term MTD is generally used for a single event in outcrop-scale studies, but which may contain more than one flow phase (Jackson et al. 2009). Alternatively, the term mass-transport complex (MTC) is commonly used in seismic interpretation, and refers to features that can only be imaged on large seismic surveys (Weimer and Shipp 2004), or when several MTDs are present but cannot clearly be distinguished from one another (Weimer and Shipp 2004).

The integration of both seismic and outcrop-based datasets have helped to improve our understanding of mass-transport processes and their distribution in deep water settings (e.g Mutti 1985; Posamentier and Kolla 2003; Martinsen et al. 2003; Dykstra et al. 2011). However, there is still a gap in scale and resolution when comparing interpretation and description of MTDs observed in seismic and outcrop datasets (e.g Mutti 1985; Posamentier and Kolla 2003; Martinsen et al. 2003; Dykstra et al. 2011). Seismic data allow full three-dimensional imaging of the sedimentary succession and may be better suited for describing large-scale features (>100 m thick), such as erosion, internal and external deformation, their relationship with each other and their lateral distribution and evolution (e.g. Prior et al. 1984; Posamentier and Kolla 2003; Bull et al. 2009; Ogata et al. 2014; Moscardelli

and Wood 2015; Alves 2015). Outcrop observations, on the other hand, are better suited to detailing small-scale information within MTDs, such as lithological distribution, structures, textures, deformation style and detailed geometries, at scales ranging from 10^{-3} to 10^{1} metres. Outcrop studies may therefore more effectively elucidate the types of processes and kinematics associated with MTD/MTC emplacement (e.g. Dykstra et al. 2011; Ogata et al. 2012; Alsop et al. 2016; Sobiesiak et al. 2016b; Alsop et al. 2017).

To date, many studies have focussed on the study of paleoslopes and consequently the inferred overall direction of movement of MTDs, using slump folds as estimators to yield downslope direction (e.g. Woodcock 1976 and 1979; Bradley and Hanson 1998; Alsop and Marco 2012). Such slump fold patterns are widely used both in seismic (e.g Bull et al. 2009) and in outcrop assessments (e.g. Alsop and Marco 2013; Alsop et al. 2016). As a slump initiates, folds may form with their axes orientated parallel to the strike of the slope i.e. up to ~90^{o} from the mean dip direction of the slope (Woodcock 1979; Strachan and Alsop 2006). As the slump translates downslope a consequent shear of stress is imposed and folds are progressively deformed, resulting in fold axes rotating within the plane of flow towards the downslope direction (e.g. Woodcock 1979; Alsop and Marco 2013).

The principal aims of this study are to provide answers to the following questions:

- What are the different styles of deformation related to MTDs in the case study and how typical are they?
- How do sandstone layers with varying thickness respond to deformation within a MTD?
- How can the main flow direction of MTDs be ascertained, and what types of kinematic indicator are observed?

In order to achieve these aims, we present structural interpretations of two contrasting MTDs, each showing a series of unique sedimentological, structural and geomorphological features that we describe in detail. The deposits are classified as either fault- or fold-dominated MTDs; the fault-dominated MTD displays a rapid transition from a compressional into an extensional domain, the latter being marked by imbricated bodies of sandstone, boudinaged sandstone blocks, and ripped-up clasts. The fold-dominated MTD is distinguished by abundant slump folds, which enable detailed

kinematic analysis of the deposit. In addition, we define five potential stages of fold evolution where asymmetric folds are the least deformed, while folds with rotated and detached hinges represent the most deformed.

2 Geological Setting

Cañon de La Peña (or simply 'La Pena') is a gorge accessible via National Road 150 (RN 150), near the western entrance of the Ischigualasto Provincial Park, and is located at the border of San Juan and La Rioja Provinces in north-western Argentina (Fig.1). La Pena is positioned towards the north-eastern margin of the Late Paleozoic Paganzo Basin (Fernandez-Seveso and Tankard 1995; Limarino et al. 2002) and is interpreted as a slope system with proglacial influence. Paganzo is an epicratonic basin that is the product of Gondwana consolidation during the Ordovician and Early Carboniferous, when three crustal terranes (Famatina, Cuyania and Chilenia), were individually accreted to the western margin of the craton (Limarino et al. 2002; Limarino et al. 2006; Desjardins et al. 2009).

According to Fernandez-Seveso and Tankard (1995), deposition in the Paganzo Basin started during the early Carboniferous, and lasted until the Late Permian. Such sediments sit unconformably on Precambrian metamorphic rocks and Ordovician sedimentary rocks that represent the basin margins. The basin was affected by at least two major post-glacial transgressive events during the Late Palaeozoic Ice ages (LPIA), which were subdivided according to post-glacial association (marine to continental facies) by Limarino et al. (2002) (see also Valdez et al in press.). La Peña is positioned where sedimentation styles change from open marine in the western domain to brackish in the eastern and central domains. Fernandez-Seveso and Tankard (1995) lithostratigraphically divided the Paganzo Group into three super-sequences; Guandacol, a 2000 m thick sequence of proglacial sediments ranging from distal turbidites, shales and MTDs with drop-stones; Tupe, a 1300 m thick sequence of fluvial, lacustrine and marine sediments; and Patquía, a 1300 m thick sequence of continental red bed sediments, fluvial facies and playa lake deposits (Fernandez-Seveso and Tankard 1995; Azcuy et al. 1999). The deposits described in this case study belong to the Guandacol super-sequence.

Cañon de La Pena is incised into the western flank of the Ischigualasto and Caballo Anca Ranges. This is part of the basement uplift eastwards of the crustal-scale Valle Fertil Fault, which was active from the Early Palaeozoic and strongly influenced sedimentation during the latter part of the Palaeozoic until the Neogene. La Peña exposes rocks from the Guandacol Formation unconformably overlain by Lower Triassic rocks. Previous mapping in the area by Milana et al. (2010) demonstrated that the sedimentary succession is dominated by at least five Carboniferous MTDs intercalated with black shale and turbidite intervals. The MTD dominated succession is over 900 m thick and is overlain by 200 m of turbidites and pro-deltaic sediments capped by Triassic red beds (Milana et al. 2010). It has been suggested that the Carboniferous paleoslope at La Peña had an irregular shape, as some MTDs suggest a transport direction towards the NNE, while others infer flow to the WNW (Milana et al. 2010).

3 MTD sedimentology and structure

We describe two MTDs that crop out along river beds at La Peña, both possessing a sandstone layer with variyng thickness that acts as a useful stratigraphic marker and records the deformational history within the deposits. According to the structures preserved within and adjacent to this sandstone layer, we have broadly classified the deposits into a stratigraphically lower fold-dominated MTD, and an upper fault-dominated MTD within the Guandacol Fm.

3.1 Fault-dominated MTD

The fault dominated MTD is exposed at locality points 1, 2, 3 and 4 on Fig. 1b. The outcrops encompass three distinctive units that can be traced confidently for about 500 m and comprise (from base to top): a heterolitic mudstone unit, that is composed of dark mudstone layers intercalated with sandstone beds (up to ~ 15 cm thick); a pebbly mudstone (debrite unit), which consists of granule to small pebble sized quartz clasts embedded in a muddy matrix; and finally, a medium to coarse grained, structureless sandstone unit, that can reach up to 7 m thick (Fig. 2). The MTD in this location is characterised by the presence of imbricated sandstones beds, marked by thrust planes dipping

towards the SW (Fig. 2 and 3a), that evolve down regional dip into large sandstone blocks embedded in a finer matrix (Fig. 2 and 4a).

Two styles of deformation are observed within the sandstone unit, (i) imbricate-dominated (Fig. 2 and 3a) and (ii) block-dominated (Fig. 2 and 4a).

3.1.1 Imbricate-dominated sandstones

The imbricate-dominated sandstones, which are ~8 m thick and can be traced laterally for over ~70 m, are characterised by a set of three thrust imbricate slices and a 'pop-up block'. The 'pop-up block' is bounded by two oppositely dipping thrusts (Fig. 3b). This structure passes into a thrust stack with an emergent imbricate fan morphology (Fig. 3a). The thrust stack is composed of three internally coherent imbricate slices, that diverge upwards from a sole or 'floor' thrust. These imbricate slices are separated by two sets of thrust planes, and are buttressed against the block-dominated portion of the deposit (Fig. 3a). The imbricated sandstone layer overlies a mudstone unit that is up to 2 m thick, and is locally injected along the thrust faults between the imbricated sands (Fig. 3a and c). The contact between the mudstone and the sandstone is irregular due to remobilization and emplacement. However, the presence of symmetric flame structures suggest that a depositional contact may be locally preserved between the sandstone and mudstone, although the flame structures could also have been formed during a later fluid scape event (Fig. 3d).

A debrite unit is situated in the uppermost portion of the mudstone, normally occurring a few centimetres below the contact between the mudstone and the overlying sandstone (Fig. 3b, d and e). The debrite is concordant with the mudstone bedding, and occurs as discontinuous bodies that locally thicken and thin. The debrite is generally thin (~4 cm) in comparison with the block-dominated described below. Additionally, brittle deformation in the form of contractional faults with a few cm of displacement propagate from the mudstone into the sandstone (Fig. 3a and c) and locally affect the debrite (Fig. 3e).

3.1.2 Block-dominated sandstone:

This unit consists of large sandstone blocks that range from 2 to 4 metres in height (vertical axis) and from 5 to 12 m in width (horizontal axis). These blocks are embedded within the debrite described above (Fig. 4a, b) and are almost entirely surrounded by a thin layer of mudstone ranging up to 30 cm in thickness. The basal contact of the blocks shows signs of interaction between the sandstone, mudstone and the debrite (e.g. irregular boundaries, downward and upwards injections, ripped-up clasts) (Fig. 4c, d, e and f) and are therefore very different from the imbricate-dominated sandstone described above.

Where sandstone blocks are positioned on top of the mudstone, it is possible to see downwards-directed injections of sandstone into the mudstone layers. The injections are shallow and the geometry resembles small apophyses or 'fingers' that range from 2 to 12 cm in length (Fig. 4c, d, e and f). Locally, thin sandy layers within the mudstone unit are folded (Fig. 4b). The short 'middle' limbs of such folds are thicker than the upper long limb, that are stretched and appear to have undergone boudinage resulting in pinch-and-swell like structures (Fig. 5a). Such folds are only found where the debrite layer is positioned below the mudstone unit. In addition, the sandstone blocks display thin seams of anastomosing mud injected upward at their base, while clusters of mud-clasts are observed at the same horizon as the seams. (Fig. 5b, c).

The debrite forms the matrix in which blocks are contained; however they also occur at the base of the deposit as discontinuous lenses that display pronounced lateral changes in thickness up to 30 cm. Locally, the debrite is injected downwards and truncates the bedding in the mudstone (Fig. 5d). The debrite also intrudes upwards into the mudstone to form dykes and diapir-like structures that deform the adjacent mud layers (Fig. 5e). These injections also spread laterally as sills that form pinch-and-swell like geometries (Fig. 5e). When the sandstone is positioned above the debrite, it is possible to see evidence of the debrite having injected upwards. The sandstone layers are locally pulled apart and boudinaged, with debrite infilling the necked areas (Fig. 5f). Such injections and intrusions erode and rip off fragments of sandstone and (more sporadically) mud, resulting in the creation of 'secondary' clasts within the debrite (Fig. 5g and h). These 'secondary' sandstone clasts

range in size from 5 up to 60 cm, with smaller clasts displaying a moderate to high sphericity, and are sub-rounded to rounded. Conversely, the larger clasts are elongate and sub angular (Fig.5g and h).

3.1.3 Structural interpretation of the fault-dominated MTD

We interpret the geometries described above to represent different processes and stages within the same deformational event (Fig. 2). The imbricate-dominated geometries have a compressional character represented by a pop-up block and the three imbricates (Fig. 2 and 3a and b). They are considered to have deformed the same continuous sand layer that was repeated and imbricated as in classic thrust geometries (e.g. Butler 1982). An alternative explanation could relate to the imbrication and 'collision' of originally separate sandstone blocks (rather than a continuous sandstone layer) due to a change to overall compression. We suggest that this is unlikely due to the similar character of each sandstone imbricate, and the lack of debrite infilling the gaps between the sandstone blocks.

The change to compressional flow may be caused by; (i) a change in rheology due to expulsion of water and/or addition of incorporated sediment (note that the frontal part of the imbricate has a high proportion of debritic injection); (ii) a change in the geometry of the basal surface from a flat into a ramp, thereby creating an accumulation zone; (iii) a change in flow behaviour where the debritic layer is absent, resulting in no 'easy-slip' or lubricating horizon.

The block-dominated geometries are more extensional in character and are translated in the form of separate sandstone blocks surrounded by mud and encased in the debrite (Fig. 2 and 4a). Such blocks also show aspect ratios (long (x) axis versus short (y) axis) of around 3 in 2D section, suggesting that they may have undergone boudinage.

Most of the sandstone blocks display mud clasts and mud seams at the base (Fig. 5b and c) and downwards injection of sand (Fig. 4c, e and f), indicative of interaction with the underlying mudstone horizon. Such features are not observed in the imbricates, suggesting two different stages of disaggregation over a relatively short distance. Additionally recumbent folds are observed below some of the blocks (Fig. 4b), suggesting that horizontal contraction also occurred. In this case, folds show a pinch-and-swell structure on the upper limb (Fig. 5a), indicating overprinting of compressional features by subsequent extension or by progressive deformation when the deformed

layer is locally oblique to the direction of shear (e.g. Van der Wateren et al. 2000; Dykstra et al. 2011; Alsop and Marco 2013).

3.1.4 Emplacement Model

Here we suggest a simple model to explain the emplacement of the fault-dominated MTD, according to field observations and the relationship between the units (Fig. 6).The fault-dominated MTD is sandwiched above and below by an intercalation of mudstones and bedded sandstone layers (heterolitic unit) that extend for at least tens of metres in both directions.

In our model, the pebbly mudstone (debrite) was deposited on top of mudstone, and this was followed by further mudstones and intercalated mudstone with thin sandstone layers. Deposition of these overlying mudstone may have trapped water within the underlying pebbly mudstone. This sequence was then 'capped' by the deposition of a thick (up to 8 m) sandstone package, that was subsequently deformed (Fig. 6).

Our model places the detachment surface at the base of the pebbly mud while the sea floor was at the top of the sand package (Fig. 6). Although the triggering mechanism for slope failure can only be inferred, the action of gravity on a rapidly deposited thick sand package that overlies a wet pebbly mud could be sufficient to create instability and cause failure. However a seismic event can not be discounted as a possible trigger.

In order to generate the deformational features described above (sandstone blocks, sandstone imbrication, sand and mud injections etc.) we assume that the mudstone and sandstone were unlithified at the time of the failure. Evidence of this is provided by interrelationships between the three units, where mud seams, clasts and sand injections are found at the base of sandstone blocks, with pebbly mudstone injecting into all units and ripping off clasts in the process. As the MTD translated downslope, the sandstone was fragmented, with blocks and individual fragments boudinaged by the flow as they sunk into the mudstone, which then wrapped around the fragments (Fig. 6a). In contrast, in the imbricate-dominated setting, the sandstone appears to have moved as a single unit, undergoing limited deformation until it was butressed and developed thrust imbrication and infilling of fault planes with mud (Fig. 6b).

The pebbly mudstone occurs as thin lenses below the imbricate-dominated sandstone and appears to be ‘squeezed out’ by the compressional character of the imbricate-dominated zone. However, downdip from the imbricates, the pebbly mudstone apparently injects upwards into the mudstone and sandstone, ripping up clasts from both units and becoming the flow matrix as it was pushed upwards (Fig. 6b).

Moreover, the propagation of brittle structures such as reactivation of thrust faults into the mudstone (Fig. 3d), and the sharp thrust contact in the pebbly mudstone below the sandstone (Fig. 3e), are suggestive of post-depositional creeping, and either a rapid change in the rheological properties of the pebbly mudstone into a rigid state, possibly due to dewatering, or a dramatic increase in strain rate. Furthermore, the turbidite sequence located below the MTD displays growth strata in the form of a fanning shape geometry of its beds, and is consistent with creeping (see Figure 13 from Kneller et al. (2016)).

3.2 Fold-dominated MTD

The fold-dominated MTD crops out beside a dry riverbed just southeast of the RN 150 road (point 5 on Fig. 1b). The exposure is up to 3 m high and is ~ 40 m long, encompassing a ~2 m thick slump unit composed of deformed mudstone with thin sandstone turbidites (up to ~1 cm thick) and an outsized (up to ~ 30 cm thick) red sandstone bed that is broken up into fragments (Fig. 7a). The MTD is overlain by an intercalation of thin sandstone and mudstone layers (up to ~2 cm), which form a ~ 18 cm thick unit that truncates the underlying folds, suggesting an erosive contact (Fig. 7b). This sequence is overlain by a further ~10 cm thick red sandstone layer, followed by a ~25 cm unit composed of thin sandstone beds (up to ~1 cm) intercalated with mudstone layers (up to ~2 cm). Finally, this local sequence is capped by a 20 cm thick pebbly mudstone layer. The main structural characteristics of the deposit are the deformed unit containing slump folds, sandstone blocks, sheared sandstone layers and internal detachments, which are now described in detail.

3.2.1 Slump Folds

The slumped unit is intensely deformed and contains thin sandstone layers deformed into SE- and NW-verging folds (Fig. 7c and d). The SE-verging folds have gently NW-dipping axial planes (mean strike and dip 061/17NW), with axial-planar strikes distributed over a limited 100° arc (Fig. 7d). The NW-verging folds are marked by gently E-dipping axial planes (mean strike and dip 000/13E) with strikes ranging over a slightly more limited 74° arc (Fig. 7d). Both fold types have hinges that plunge at shallow angles towards the ~NNE (mean 036°), with hinge trends distributed over a 48° arc (Fig. 7d).

In general, the folds are asymmetric and are marked by the development of upright folds (early stages) through to progressively inclined asymmetrical fold (later stages), suggesting potential modification by progressive simple shear (Alsop and Marco, 2013). Such asymmetrical folds display long, stretched and thinner limbs, interpreted to lie in the extensional field, while shorter and thicker limbs lie in the contractional field of the strain ellipse (Fig. 7c).

Additionally, asymmetric, doubly-vergent folds that resemble a box-fold geometry occur within the slump horizon, with two sets of axial planes for each hinge located in the ‘edges of the box’ (Fig. 7e). These axial planes dip in opposite directions and converge downwards towards a single point. The large doubly-vergent fold in the La Pena slump is bounded by two shear planes, one of which entirely truncates the upper limb of the fold, while the other stretches and thins the lower limb (Fig. 7e). The box fold geometries are interpreted as detachment folds, and are the result of buckling above an easy-slip horizon where the detachment propagates (Fossen 2010; Alsop and Marco 2013).

3.2.2 Slump fold evolution

It is possible to recognise five general stages of fold evolution within the slumped interval. These stages are; (i) asymmetric folds, described in section 3.1.1, (ii) folds with incipient shearing, characterized by an increase in thickness of the upper limb towards the hinge, where the maximun thickness (~20 cm) is attained. The lower limb is shorter in length (~10 cm) and very thin (~2 cm); (iii) sheared fold limbs, characterized by the presence of only one limb (upper or lower) which shows different degrees of shearing by the flow, preserving the hinge (where the bulk of the sand is found); (iv) limbless folds, characterized by the presence of an ellipse-shaped hinge and the vestige of one

sheared limb; (v) rotated and detached hinges, where rounded sandstone blocks deform the bed around it as if they were rotating (Fig. 8a and b). This sequence is generally considered to relate to an increase in overall shear strain within the slumped unit.

The least deformed end member is represented by (i) asymmetrical folds (Fig. 7c and 8b) as described above, which are recumbent and characterized by a longer and thinner limb adjacent to a shorter and thicker limb. As flow progresses, shear strain increases and internal detachments start to develop. These truncate the folds and cut the short limbs of the fold close to the fold hinges achieving the second stage (ii), incipient shearing (Fig.8b and c). Following that, the shear surfaces evolve, resulting in the offset of one of the limbs, leaving only the fold hinge and the other limb, forming the third stage (iii), sheared fold limbs (Fig. 8b and d). As hinges gradually start to rotate, fold limbs begin to show signs of shearing and attenuation as they start to thin and fade into the matrix, with only part of the fold surviving as a rounded body of sand (iv),forming a limbless fold (Fig.8b and c). Finally, the most deformed end-member (v) hinge rotation is the severed fold hinge that behaves as a block and rotates within the flow thereby deforming the strata around it (Fig.8b and e).

3.2.3 Outsized sandstone layer

The fold-dominated MTD contains several fragments of an outsized sandstone bed of variable thickness (up to ~30 cm) that are preserved as slabs and blocks, discriminated by aspect ratio; the slabs are up to ~15 cm thick and up to ~2.5 m long, while blocks can be up to ~30 cm thick and 55 cm long. Such slabs are scattered throughout the deposit and appear to be derived from more than one outsized bed, because individual single slabs are mostly found in the upper part of the slump unit, while continuous and sheared slabs and blocks are aligned along the same horizon (as if they were originally a single bed) in the lower part of the slump (Fig. 8a).

Slabs in the upper part of the slump are broken into smaller pieces up to ~50 cm long that show weak internal deformation and attenuated edges when compared to slabs from the lower part. Such attenuation may indicate that the flow was interacting with the slab in a more abrasive way, or suggest that the difference in competence between the flow matrix and the sand slab was forcing the slab to undergo boudinage by the flow. Where larger slabs are folded, the thickness of the deformed sand

layer is greater in the fold hinge and gets progressively thinner towards the limbs (Fig. 7c). Such structures may result from progressive simple shear of a competent layer, where buckling and folding are followed by unfolding, stretching and boudinage of fold hinges and limbs as simple shear proceeds (Van der Wateren et al. 2000). In some cases, the outsized sandstone layer can be found as rounded bodies of sand or blocks (Fig. 8e).

Sand slabs and blocks in the lower part of the slumped unit are all located along the same horizon, which acts as a marker for thrust planes that offset the layer (Fig. 8a and d). The slabs in the lower part, which are very similar to those described above from the upper part, are rectangular shaped, weakly deformed and sheared. Attenuated edges rapidly disintegrate into a thin (~ 2 cm) seam of sand-rich matrix that connects to another slab or block. Although blocks have a variable shape, they all share an ellipsoid geometry, and are thicker than the slabs described above (Fig. 8c and d)

4 Kinematic Indicators

An array of kinematic indicators can be used from each MTD within La Pena to determine overall movement direction. The fault-dominated MTD displays thrust fault imbrication, with thrust planes dipping towards ~ 247°, which when taken together with measurements from associated fold hinges, suggests a mean transport directions towards the NE (067°). Fold hinge and axial plane data collected from the fold-dominated MTD (Fig. 7d) shows fold hinges distributed into two populations of SE- and NW- verging folds. The separation arc method developed by Hansen (1971) is not appropriate in this case as there is no distinct angle of separation between the two population of SE and NW verging folds. We have therefore applied the Axial-planar Intersection method (AIM of Alsop and Marco 2012) and this suggests an overall transport direction towards ~ 036°.

In order to better constrain the overall transport direction, we also gathered structural data from a separate debritic interval. This interval is located a couple of metres below the fold-dominated MTD (point 6 on Fig. 1b), and is composed of a debrite containing numerous mud clasts (Fig. 9a). We measured the orientation of the long axes of the mud-clasts, as exposed on bedding planes, and they are orientated towards ~ 040° and interpreted as lying parallel to the NE-directed transport direction

(Fig. 9b). In summary, we have used three different techniques to determine transport direction, and all three deposits provide similar flow directions. We are therefore confident that the main flow direction within this part of the basin, at least for the studied intervals, was towards the NE.

5 Axial planar cleavage in slump folds

A spaced axial planar cleavage is recognised in slump folds in a horizon located several metres below the fold-dominated MTD (point 7 on Fig. 1b). In this horizon, the slump folds are predominantly SE-verging and show mm-scale crenulation cleavage and fracture cleavage that is approximately parallel to the fold axial plane (Fig. 9c and d). It is important to note that the beds above and below this slumped horizon do not display such a fabric. Axial planar cleavage is now interpreted to form during slumping (see discussion in Alsop and Marco, 2014) as well as in other soft-sediment settings (see also Alterman 1973; Beutner et al. 1977; Dykstra 2005; Meere et al. 2016). The development of axial planar cleavage within slump folds is thus entirely consistent with the syn-depositional origin for these structures.

6 Discussion

6.1 Fault-dominated MTD

6.1.1 Liquidization

Liquidization is a term that simply describes any process that transforms sediments from a solid into a fluid like state, and is a primary process in downslope mobilization of unconsolidated or partially-consolidated sediments (e.g. Allen 1982; Owen 1987; Maltman and Bolton 2003). Liquidization occurs when sediment grains are supported by pore-fluid rather than intergranular contact, causing a loss of shear strength with the sediment effectively behaving as a fluid (Maltman and Bolton 2003). Liquidization can be divided into fluidization and liquefaction. Fluidization is when the sediments behave as a liquid by the flow of pore fluids that suspends the grains, (e.g. Urquhart; Nichols 1995; Zhu et al. 2005). Liquefaction develops when any additional load on a sediments is completely suported by pore-fluid, causing the grains to become suspended, therefore losing strength

and cohesion and starting to behave like a fluid (Andresen and Bjerrum 1967; Lowe 1975; Hampton et al. 1996).

As suggested above (section 3.1.4), the additional load caused by the deposition of sand, or another trigger mechanism, caused the debrite to become unstable. The debrite transformed into a liquid-like state by one or more of the processes described in the paragraph above leading to downslope failure, with the sands sinking into the liquefied debrite. As the MTD translated downslope, the sand layer was fragmented and deformed by the flow. The fragments that have a blocky shape show evidence of layer-parallel extension, as they are more competent than the surrounding debrite and undergo boudinage. In contrast, the imbricate-dominated sandstone shows no signs of liquidization.

Additionally, in a fluidized sediment pore fluid is expelled towards areas of lower fluid pressure, which in most cases is upwards (Lowe 1975; Maltman and Bolton 2003). Such migration of fluid and sediment is shown by intrusions in the form of clastic injections (Peterson 1968; Hiscott 1979), even in areas undergoing contractional deformation (e.g. Palladino et al. 2016). Indication of such process in the studied sucession are the upwards injection of debrite into the mudstones as dykes and diapir-like features (Fig. 5e and f). However, such injections can locally be in any direction, including downwards (e.g. Peterson 1968; Hiscott 1979; Huang 1988), exactly as shown by the downwards injecting debrite (Fig. 5d) and sandy injections (Fig. 4c, e and f) intruding the mudstones and the lateral debritic sill-like intrusions. The downwards pointing sand injections suggest that the sandstone blocks were also liquified; the same assumption can be applied to the mud clasts and seams found at the base of the sandstone blocks, where the mud clast would result from the erosion of the underlying mud horizon, and the mud seams from its upward injection. On the other hand, the sandstone blocks were undergoing shear-stripping, as mudstone and sandstone clasts were ripped out and incorporated into the matrix (Fig. 5g and h). Such clasts show a rigid behaviour rather than liquid-like, and the physical state of the sandstone blocks is therefore complex and varies along the MTD.

Comparing the structures observed in the fault-dominated MTD with the structures described and interpreted by Strachan (2002), suggests that liquefaction was the major process acting on the MTD. Thus, fluidization generated the intrusions and liquefaction generated the folds.

6.1.2 Thrust faults (compressional)

Thrust systems in MTDs have been widely described from seismic (e.g. Bull et al. 2009; Posamentier and Martinsen 2011) and outcrop data (e.g. Farrell 1984; Dykstra et al. 2011; Alsop et al. 2017) and their surface expressions are usually referred to as pressure ridges. Such features are the result of heterogeneous shear, and normally generate a classic duplex and imbricate geometry (Frey Martinez et al. 2006; Bull et al. 2009; Posamentier and Martinsen 2011). These structures typically affect the entire thickness of the MTD, and are commonly described from the most distal region or "toe domain" of the flow (e.g. Frey Martinez et al. 2006; Bull et al. 2009). However, thrusts can also develop at the lateral margins of a flow, around any obstacle to a flow (e.g. remnant and rafted blocks, salt diapirs etc), or due to localised variations in topography as the basal shear surface cuts up to a shallower stratigraphical horizon, thus creating a zone of flow accumulation and horizontal shortening (e.g. Gawthorpe and Clemmey 1985; Bull et al. 2009).

In seismic sections, thrusts are characteristically expressed as discontinuity between offset reflections, in many cases, this discontinuity would have a listric form dipping at least ~15° but potentially steeper. They are considered to originate at the base of the MTD and extend through the deposit to its upper surface where they commonly create topography (e.g. Kneller et al. 2016). Normally, reflections associated with thrusts dip upslope, however downslope dipping thrusts occasionally occur and are often interpreted as back thrusts related to larger synthetic thrusts (Martinsen and Bakken 1990). In plan-view, thrusts occur as arcuate lines that are convex in the downslope direction, even when they display a back thrust sense.

Using field data from western Ireland Martinsen and Bakken (1990) describe imbricate thrusts with a sheared mud horizon infilling the gap between the thrust slices from a slump and a slide section. In plan-view, each thrust is described as a convex lobe of sediment piled on top of another and separated by the sheared mudstone. This thrust system is structurally and sedimentologically very similar to the imbricate-dominated sandstone, where imbricated thrust slices are separated by sheared mudstone (section 3.1.1). Huvenne et al. (2002) analysed 2D and 3D seismic data showing a frontally confined MTD (sensu Frey-Martínez et al. (2006)) containing undisturbed blocks in the western Porcupine Basin, Ireland. They describe the occurrence of elongate blocks orientated perpendicular to

the main shortening direction in the frontal thrust system. Some of the blocks were tilted and thrusted, and internal stratification could not be detected, unlike blocks elsewhere within the deposit.

We suggest that these two examples may help explain how the imbricate-dominated sandstone observed in our study area was developed. It could have been formed where a compositionally heterogeneous MTD was buttressed against an obstacle to the flow, leading to compression and formation of thrust imbricates (e.g. Martinsen and Bakken 1990). Alternatively, blocks may have been aligned perpendicular to the flow and buttressed against each other, resulting in thrust faults filled by the sheared matrix (Huvenne et al. 2002). Based on our field observations, we suggest that that the sandstone layer was buttressed against an obstacle to the flow leading to the development of thrust faults.

6.1.3 Blocks (extensional)

MTDs containing coherent rafted blocks are widely documented in the literature from both seismic (e.g. Bull et al. 2009; Jackson 2011; Olafiranye et al. 2013; Alves 2015) and outcrop data (e.g. Macdonald et al. 1993; Lucente and Pini 2003; Dykstra et al. 2011; Sobiesiak et al. 2016a and b). They are usually interpreted as pieces of coherent stratigraphy that experience little or no internal deformation, and are derived either from the fragmentation of the MTD protolith, from erosion of the substrate, or both.

According to Alves (2015), blocks in seismic data are distinguished as features with high reflection strength, in comparison with the variable amplitude of the disrupted strata of the MTD matrix. They are generally classified as either remnant or rafted blocks, with remnant blocks showing continuity with the underlying non-MTD strata, while rafted blocks ‘float’ within the matrix, or rest on top of a glide surface that has transported them downslope (Alves 2015).

Dykstra et al. (2011), Garyfalou (2015) and Sobiesiak et al. (2016a and b) described a blocky MTD from Cerro Bola, NW Argentina, that contains sandstone blocks derived by erosion of the basal shear surface that were incorporated into the moving flow. Such sandstone blocks are interpreted to have been unlithified at the time of incorporation and are generally structureless, with signs of fragmentation by stretching and boudinage resulting in an eye-shaped geometry. It is also possible to interpret material having been sheared from the blocks and incorporated into the matrix.

458 The blocks described above in section 3.1.2 are floating within the MTD matrix, show no vertical
459 continuity with underlying stratigraphy, and can therefore be classified as rafts according to Alves
460 (2015). Such blocks show similar features and geometries to those described by Sobiesiak et al.
461 (2016a, and b), with both having eye-shaped geometries, indicative of boudinage of the sandstone
462 layer. Another similar feature is the abrasion of the material from the blocks and its incorporation into
463 the matrix of the flow (Garyfalou 2015; Sobiesiak et al. 2016b). In the Cerro Bola example, the sand
464 material sheared from the blocks behaves in a more ductile style (with sand blebs and stringers
465 resulting in a sand rich matrix) compared with the sandstone clasts from La Pena. This may be
466 indicative of the degree of lithification prior to deformation.

467 **6.2 Fold-dominated MTD**

468 **6.2.1 Fold generation within a slump**

469 Slumps are most simply described as a single downslope moving cell, containing extension at the
470 upper end, termed the headwall domain, contraction at the lower downslope end termed the toe
471 domain, and a translational domain between these two where the slump moves downslope over a
472 detachment surface (e.g. Farrell, 1984; Bull et al. 2009).

473 According to Alsop and Holdsworth (2007), fold geometry and orientation are generally
474 governed by how displacement occurs on the underlying detachement surface (e.g. Coward and Potts
475 1983). Layer-parallel shear (LPS) develops where displacement is constant and parallel to the slump
476 direction, producing quasi-cylindrical folds at a high angle to flow and unimodal fold facing patterns
477 sub-parallel to flow direction. Conversely, layer-normal shear (LNS) forms when the displacement is
478 non-constant leading to differential movement, producing cylindrical folds oblique or even parallel to
479 flow, and a bimodal fold facing pattern at a high angle to flow direction (Alsop and Holdsworth 1993;
480 Alsop and Holdsworth 2007). The non-constant displacements of LNS produce localized flow
481 perturbation resulting in zones with a relative acceleration (surging flow) and deceleration (slackening
482 flow) in comparizon with the background velocity. According to Alsop and Holdsworth, (2007), an
483 accelerating flow perturbation develops an antiformal culmination, where the arc of hinge-line
484 curvature closes in the direction of transport. Conversely, in a decelerating flow perturbation, a

485 synformal depression forms, wih the arc of hinge-line curvature opening in the transport direction
486 (Fig. 10).
487 The slump fold geometries and style described in the fold-dominated MTD are very similar to
488 the LNS pattern describe above from Alsop and Holdsworth (2007). The bimodal fold vergence
489 distribution and facing pattern, the oblique asymmetric (Z and S) type of folding developed sub-
490 parallel to flow, and the axial planes dipping in opposite directions are all consistent with LNS-
491 dominated flow (Fig 10a and b). The development of thrust faults which strike sub-parallel to inferred
492 flow, and with displacements directed away from one another, together with the mean axial plane and
493 the clustering of fold hinges of the SE and NW verging folds, all suggest that the fold hinges diverge
494 away from one another in a downflow direction (Fig 7d). Thus, the overall geometry of the faults plus
495 the deformation and offset of the outsized sandstone bed clearly demonstrate a depression surface
496 flanked by culminations. The overall behaviour of the flow is therefore consistent with a depression
497 surface in the LNS model (Fig 10a and b) (Alsop and Holdsworth 1993; Alsop and Holdsworth 2007).
498

499 # 7 Conclusions

500 In this paper we have described and discussed two sub-seismic scale examples from the Late
501 Carboniferous Paganzo basin, which we classified as fault- and fold-dominated MTDs. The fault-
502 dominated MTD is characterized by the lateral change, over a few 10's of metres, from sets of
503 imbricated sandstone slices (compressional) into individual sets of sandstone blocks (extensional),
504 which are both embedded in a debrite unit. The debritic unit itself shows signs of liquidization,
505 resulting in the overlying mudstone and sandstone units sinking into it, and ripping up pieces of
506 sandstone and mudstone in the process. Upwards injection of debrite as diapir-, sill- and dyke-like
507 structures can be seen, as well as downwards injection of sandstone and debrite into the substrate. The
508 sandstone blocks also possess clusters of mud-clasts and mud-seams anastomosing at the base.
509 The fold-dominated MTD contains bimodal fold vergence and facing patterns, oblique
510 asymmetric (Z and S) type of folding developed sub-parallel to flow, and axial planes dipping in

opposite directions which are all consistent with LNS-dominated flow towards the NE. The development of thrust faults, which strike sub-parallel to NE-directed flow and with displacements directed away from one another, suggests that there may be a component of convergent flow on each flank of the depression. Additionally, five stages of fold evolution are noted, starting with asymmetrical folds, which as flow progresses become sheared untill the hinges become detached and rotate as ‘blocks’ thereby deforming their immediate surroundings.

Overall, we can conclude that thin (i.e. up to ~ 30 cm) and thick (i.e. up to 4 m) sandstone beds respond differently to deformation. Thin beds tend to fold with variations in flow, while thick beds have the tendency to develop longer wave-length folds and thrust zones. As such, systems of thrusts and blocks affecting thicker beds are more apparent in seismic analysis. Folding is generally unresolvable on seismic sections and may form below the limits of resolution and/or be too tight to be clearly imaged. In summary, outcrop description and observation of geometries, architecture and structural relationships of MTDS are vital for a detailed lithological and deformational understanding, which is not achievable through seismic analysis alone.

Acknowledgments

This work was carried out with support from CNPq (Conselho Nacional de Desenvolvimento Científico e Tecnológico) - Brazil, BG - Brazil and the University of Aberdeen. We would like to thank the following geologists for their support, camaraderie and countless hours of fieldwork: Arthur Giovannini, Claus Fallgatter, Victoria Valdez, Qun Liu, Carla Puigdomenech, Guilherme Bozetti and Roberto Noll Filho. We thank Christopher Jackson and an anonymous reviewer, whose constructuve comments and criticism helped to improve the manuscript.

References

Allen JRL (1982) Sedimentary Structures: Their Character and Physical BasisPhysical Basis, Elsevier, Amsterdam, 663 pp.

Alsop GI, Holdsworth RE (1993) The distribution, geometry and kinematic significance of Caledonian buckle folds in the western Moine Nappe, northwestern Scotland. Geol Mag 130:353. doi: 10.1017/S0016756800020033

Alsop GI, Holdsworth RE (2007) Flow perturbation folding in shear zones. Geol Soc London, Spec Publ 272:75–101. doi: 10.1144/GSL.SP.2007.272.01.06

Alsop GI, Marco S (2012) A large-scale radial pattern of seismogenic slumping towards the Dead Sea Basin. J Geol Soc London 169:99–110. doi: 10.1144/0016-76492011-032

Alsop GI, Marco S (2013) Seismogenic slump folds formed by gravity-driven tectonics down a negligible subaqueous slope. Tectonophysics 605:48–69. doi: 10.1016/j.tecto.2013.04.004

Alsop GI, Marco S (2014) Fold and fabric relationships in temporally and spatially evolving slump systems: A multi-cell flow model. J Struct Geol 63:27–49. doi: 10.1016/j.jsg.2014.02.007

Alsop GI, Marco S, Levi T, Weinberger R (2017) Fold and thrust systems in Mass Transport Deposits. J Struct Geol 94:98–115. doi: 10.1016/j.jsg.2016.11.008

Alsop GI, Marco S, Weinberger R, Levi T (2016) Sedimentary and structural controls on seismogenic slumping within mass transport deposits from the Dead Sea Basin. Sediment Geol. doi: 10.1016/j.sedgeo.2016.02.019

Alterman IB (1973) Rotation and Dewatering during Slaty Cleavage Formation: Some New Evidence and Interpretations. Geology 1:33. doi: 10.1130/0091-7613(1973)1<33:RADDSC>2.0.CO;2

Alves TM (2015) Submarine slide blocks and associated soft-sediment deformation in deep-water basins: A review. Mar Pet Geol 67:262–285. doi: 10.1016/j.marpetgeo.2015.05.010

Andresen A, Bjerrum L (1967) Slides in subaqueous slopes in loose sand and silt. Mar Geotech 221–239.

Azcuy C, Carrizo H a., Caminos R (1999) Carbonífero y Pérmico de las Sierras Pampeanas, Famatina, Precordillera, Cordillera Frontal y Bloque de San Rafael.

560 Beutner EC, Jancin MD, Simon RW (1977) Dewatering origin of cleavage in light of deformed calcite
561 veins and clastic dikes in Martinsburg slate, Delaware Water Gap, New Jersey. Geology 5:118.
562 doi: 10.1130/0091-7613(1977)5<118:DOOCIL>2.0.CO;2
563 Bradley D, Hanson L (1998) Paleoslope Analysis of Slump Folds in the Devonian Flysch of Maine. J
564 Geol 106:305–318. doi: 10.1086/516024
565 Bull S, Cartwright J, Huuse M (2009) A review of kinematic indicators from mass-transport
566 complexes using 3D seismic data. Mar Pet Geol 26:1132–1151. doi:
567 10.1016/j.marpetgeo.2008.09.011
568 Butler RWH (1982) The terminology of structures in thrst belts. J Struct Geol 4:239–245.
569 Coward MP, Potts GJ (1983) Complex strain patterns developed at the frontal and lateral tips to shear
570 zones and thrust zones. J Struct Geol 5:383–399. doi: 10.1016/0191-8141(83)90025-1
571 De Blasio F V., Ilstad T, Elverhøi A, et al (2013) High Mobility Of Subaqueous Debris Flows And
572 The Lubricating-Layer Model. In: Offshore Technology Conference. Offshore Technology
573 Conference, pp 1–11
574 Desjardins PR, Buatois L a., Limarino CO, Cisterna G a. (2009) Latest Carboniferous–earliest
575 Permian transgressive deposits in the Paganzo Basin of western Argentina: Lithofacies and
576 sequence stratigraphy of a coastal-plain to bay succession. J South Am Earth Sci 28:40–53. doi:
577 10.1016/j.jsames.2008.10.003
578 Dykstra M (2005) Dynamics of Submarine Sediment Mass-Transport, from the Shelf to the Deep Sea.
579 UNIVERSITY OF CALIFORNIA
580 Dykstra M, Garyfalou K, Kertznus V, et al (2011) Mass-Transport Deposits: Combining outcrop
581 studies and seismic forward modeling to understand lithofacies distributions, deformation, and
582 their seismic expression. SEPM Spec Publ 95:1–25.
583 Farrell S (1984) A dislocation model applied to slump structures, Ainsa Basin, South Central
584 Pyrenees. J Struct Geol 73:727–736. doi: http://dx.doi.org/10.1016/0191-8141(84)90012-9
585 Felix M, Peakall J (2006) Transformation of debris flows into turbidity currents: mechanisms inferred
586 from laboratory experiments. Sedimentology 53:107–123. doi: 10.1111/j.1365-
587 3091.2005.00757.x

588 Fernandez-Seveso F, Tankard AJ (1995) Tectonics and Stratigraphy of the Late Paleozoic Paganzo
589 Basin of Western Argentina and its Regional Implications. Pet Basins South Am 285–301.
590 Fossen H (2010) Structural Geology. Cambridge University Press
591 Frey-Martínez J, Cartwright J, James D (2006) Frontally confined versus frontally emergent
592 submarine landslides: A 3D seismic characterisation. Mar Pet Geol 23:585–604. doi:
593 http://dx.doi.org/10.1016/j.marpetgeo.2006.04.002
594 Gamberi F, Rovere M, Marani M (2011) Mass-transport complex evolution in a tectonically active
595 margin (Gioia Basin, Southeastern Tyrrhenian Sea). Mar Geol 279:98–110. doi:
596 10.1016/j.margeo.2010.10.015
597 Garyfalou K (2015) Integrated analysis of mass-transport deposits: Outcrop, 3D seismic interpretation
598 and fast fourier transform. Unpublished PhD thesis, University of Aberdeen
599 Gawthorpe RL, Clemmey H (1985) Geometry of submarine slides in the Bowland Basin (Dinantian)
600 and their relation to debris flows. J Geol Soc London 142:555–565. doi:
601 10.1144/gsjgs.142.3.0555
602 Hampton MA, Lee HJ, Locat J (1996) Submarine landslides. Rev Geophys 34:33–59. doi:
603 10.1029/95RG03287
604 Hansen E (1971) Strain Facies. Springer Berlin Heidelberg, Berlin, Heidelberg
605 Haughton PDW, Barker SP, McCaffrey WD (2003) "Linked" debrites in sand-rich turbidite systems -
606 origin and significance. Sedimentology 50:459–482. doi: 10.1046/j.1365-3091.2003.00560.x
607 Hiscott RN (1979) Clastic Sills and Dikes Associated with Deep-Water Sandstones, Tourelle
608 Formation, Ordovician, Quebec. SEPM J Sediment Res Vol. 49:1–9. doi: 10.1306/212F76A3-
609 2B24-11D7-8648000102C1865D
610 Huang Q (1988) Geometry and tectonic significance of Albian sedimentary dykes in the Sisteron area,
611 SE France. J Struct Geol 10:453–462. doi: 10.1016/0191-8141(88)90033-8
612 Huvenne VAI, Croker PF, Henriet J-P (2002) A refreshing 3D view of an ancient sediment collapse
613 and slope failure. Terra Nov 14:33–40. doi: 10.1046/j.1365-3121.2002.00386.x
614 Jackson CA-L (2011) Three-dimensional seismic analysis of megaclast deformation within a mass
615 transport deposit; implications for debris flow kinematics. Geology 39:203–206. doi:

10.1130/G31767.1

Jackson CA-L, Zakaria AA, Johnson HD, et al (2009) Sedimentology, stratigraphic occurrence and origin of linked debrites in the West Crocker Formation (Oligo-Miocene), Sabah, NW Borneo. Mar Pet Geol 26:1957–1973. doi: 10.1016/j.marpetgeo.2009.02.019

Kneller B, Dykstra M, Fairweather L, Milana JP (2016) Mass-transport and slope accommodation: Implications for turbidite sandstone reservoirs. Am Assoc Pet Geol Bull 100:213–235. doi: 10.1306/09011514210

Limarino C, Tripaldi A, Marenssi S, Fauqué L (2006) Tectonic, sea-level, and climatic controls on Late Paleozoic sedimentation in the western basins of Argentina. J South Am Earth Sci 22:205–226. doi: 10.1016/j.jsames.2006.09.009

Limarino CO, Césari SN, Net LI, et al (2002) The Upper Carboniferous postglacial transgression in the Paganzo and Río Blanco basins (northwestern Argentina): facies and stratigraphic significance. J South Am Earth Sci 15:445–460. doi: 10.1016/S0895-9811(02)00048-2

Lowe DR (1975) Water escape structures in coarse-grained sediments. Sedimentology 22:157–204. doi: 10.1111/j.1365-3091.1975.tb00290.x

Lucente CC, Pini GA (2003) Anatomy and emplacement mechanism of a large submarine slide within a Miocene foredeep in the northern Apennines, Italy: a field perspective. Am J Sci 303:565–602.

Macdonald DIM, Moncrieff ACM, Butterworth PJ (1993) Giant slide deposits from a Mesozoic fore-arc basin, Alexander Island, Antarctica. Geology 21:1047–1050. doi: 10.1130/0091-7613(1993)021<1047:GSDFAM>2.3.CO;2

Maltman AJ, Bolton A (2003) How sediments become mobilized. Subsurf Sediment Mobilization 216:9–20. doi: 10.1144/GSL.SP.2003.216.01.02

Martinsen OJ, Bakken B (1990) Extensional and compressional zones in slumps and slides in the Namurian of County Clare, Ireland. J Geol Soc London 147:153–164. doi: 10.1144/gsjgs.147.1.0153

Martinsen OJ, Lien T, Walker RG, Collinson JD (2003) Facies and sequential organisation of a mudstone-dominated slope and basin floor succession: the Gull Island Formation, Shannon Basin, Western Ireland. Mar Pet Geol 20:789–807. doi: 10.1016/j.marpetgeo.2002.10.001

644 Meere PA, Mulchrone KF, McCarthy DJ, et al (2016) Prelithification and synlithification tectonic
645 foliation development in a clastic sedimentary sequence. Geology 44:291–294. doi:
646 10.1130/G37587.1
647 Milana JP, Kneller B, Dykstra M (2010) Mass-Transport Deposits and Turbidites, Syn-to-Post-Glacial
648 Carboniferous Basins of Western Argentina. ISC 2010 F Guid 01–88.
649 Mohrig D, Marr JG (2003) Constraining the efficiency of turbidity current generation from submarine
650 debris flows and slides using laboratory experiments. Mar Pet Geol 20:883–899. doi:
651 10.1016/j.marpetgeo.2003.03.002
652 Moscardelli L, Wood L (2008) New classification system for mass transport complexes in offshore
653 Trinidad. Basin Res 20:73–98. doi: 10.1111/j.1365-2117.2007.00340.x
654 Moscardelli L, Wood L (2015) Morphometry of mass-transport deposits as a predictive tool. Geol Soc
655 Am Bull 128:B31221.1. doi: 10.1130/B31221.1
656 Mutti E (1985) Turbidite Systems and Their Relations to Depositional Sequences. In: Provenance of
657 Arenites. Springer Netherlands, Dordrecht, pp 65–93
658 Nemec W (1990) Aspects of Sediment Movement on Steep Delta Slopes. In: Colella A, Prior DB
659 (eds) Coarse-Grained Deltas. Blackwell Publishing Ltd., Oxford, UK, pp 29–73
660 Nichols RJ (1995) The liquification and remobilization of sandy sediments. Geol Soc London, Spec
661 Publ 94:63–76. doi: 10.1144/GSL.SP.1995.094.01.06
662 Ogata K, Mountjoy JJ, Pini G a., et al (2014) Shear zone liquefaction in mass transport deposit
663 emplacement: A multi-scale integration of seismic reflection and outcrop data. Mar Geol 1–15.
664 doi: 10.1016/j.margeo.2014.05.001
665 Ogata K, Mutti E, Pini GA, Tinterri R (2012) Mass transport-related stratal disruption within
666 sedimentary mélanges: Examples from the northern Apennines (Italy) and south-central
667 Pyrenees (Spain). Tectonophysics 568–569:185–199. doi: 10.1016/j.tecto.2011.08.021
668 Olafiranye K, Jackson CA-L, Hodgson DM (2013) The role of tectonics and mass-transport complex
669 emplacement on upper slope stratigraphic evolution: A 3D seismic case study from offshore
670 Angola. Mar Pet Geol 44:196–216. doi: 10.1016/j.marpetgeo.2013.02.016
671 Owen G (1987) Deformation processes in unconsolidated sands. Geol Soc London, Spec Publ 29:11–

672 24. doi: 10.1144/GSL.SP.1987.029.01.02
673 Palladino G, Grippa A, Bureau D, et al (2016) Emplacement of sandstone intrusions during
674 contractional tectonics. J Struct Geol 89:230–249. doi: 10.1016/j.jsg.2016.06.010
675 Peterson GL (1968) Flow structures in sandstone dikes. Sediment Geol 2:177–190. doi:
676 10.1016/0037-0738(68)90024-9
677 Posamentier HW, Kolla V (2003) Seismic Geomorphology and Stratigraphy of Depositional Elements
678 in Deep-Water Settings. J Sediment Res 73:367–388. doi: 10.1306/111302730367
679 Posamentier HW, Martinsen OJ (2011) The Character and Genesis of Submarine Mass-Transport
680 Deposits: Insights from Outcrop and 3D Seismic Data. In: Mass-Transport Deposits in
681 Deepwater Settings. SEPM (Society for Sedimentary Geology), pp 7–38
682 Prior DB, Bornhold BD, Johns MW (1984) Depositional characteristcs of a submarine debris flow. J
683 Geol 92:707–727. doi: 00221376
684 Sobiesiak MS, Kneller B, Alsop GI, Milana JP (2016a) Internal deformation and kinematic indicators
685 within a tripartite mass transport deposit, NW Argentina. Sediment Geol 344:364–381. doi:
686 10.1016/j.sedgeo.2016.04.006
687 Sobiesiak MS, Kneller B, Alsop GI, Milana JP (2016b) Inclusion of Substrate Blocks Within a Mass
688 Transport Deposit: A Case Study from Cerro Bola, Argentina. In: Lamarche G, Mountjoy J, Bull
689 S, et al. (eds) Submarine Mass Movements and Their Consequences, 7th international
690 symposium. Advance in Natural and Technological Hazards Research, Springer, The
691 Netherlands. Springer International Publishing, Cham, pp 487–496
692 Stow DA V (1986) Deep clastic seas, in H. G. Reading, ed., Sedimentary Environments and Facies.
693 Blackwell Sci Publ 615.
694 Strachan LJ (2002) Slump-initiated and controlled syndepositional sandstone remobilization: An
695 example from the Namurian of county Clare, Ireland. Sedimentology 49:25–41. doi:
696 10.1046/j.1365-3091.2002.00430.x
697 Strachan LJ, Alsop GI (2006) Slump folds as estimators of palaeoslope: a case study from the
698 Fisherstreet Slump of County Clare, Ireland. Basin Res 18:451–470. doi: 10.1111/j.1365-
699 2117.2006.00302.x

Urquhart W (1990). Fluidised Bed Combustion - A Review Of Current Position. Trans Inst Eng Shipbuild Scotl 129:(Parts 1-8).

Valdez V, Di Pascuo M, Milana JP, Kneller B, Fallgatter C, Paim P. (in press) Integrated U-Pb zircon and palynological/palaeofloristic age determinations of a Bashkirian palaeovalley fill, Quebrada Grande (Western Argentina).

Van der Wateren FM, Kluiving SJ, Bartek LR (2000) Kinematic indicators of subglacial shearing. Geol Soc London, Spec Publ 176:259–278. doi: 10.1144/GSL.SP.2000.176.01.20

Weimer P, Shipp C (2004) Mass Transport Complex: Musing on Past Uses and Suggestions for Future Directions. In: Proceedings of Offshore Technology Conference. The Offshore Technology Conference, pp 1–10

Woodcock NH (1976) Structural style in slump sheets: Ludlow Series, Powys, Wales. J Geol Soc London 132:399–415. doi: 10.1144/gsjgs.132.4.0399

Woodcock NH (1979) The use of slump structures as palaeoslope orientation estimators. Sedimentology 26:83–99.

Zhu J, Leckner B, Cheng Y, Grace J (2005) Fluidized Beds. In: Crowe C (ed). CRC Press, pp 5-1-5–93

Figure Captions

Fig 1: (a) Outline map of South America, highlighting Argentina. Red rectangle marks location of the field area. (b) Google Earth image of "Quebrada de la Pena" showing outcrop locations. Positions of fault-dominated MTD (red circles 1, 2, 3, and 4), fold-dominated MTD (blue circle 5), debrite with mud clasts (blue circle 6) and slump folds with axial planar cleavage (blue circle 7) localities are highlighted. The route of highway RN150 is shown for reference.

Fig 2: (a) Summary cartoon showing the lateral distribution of key outcrops (points 1 to 4 on Fig. 1b). Note the lateral variation from the imbricate-dominated (compressional) into block-dominated (extensional) domains. (b) Three schematic logs showing the vertical disposition of all three units according to their structural domain (imbricate- and block-dominated). Location is shown in Fig. 2a.

Fig 3: (a) Photo (oblique to the inferred transport direction), showing the overall imbricate-dominated sandstone and the transition into block-dominated sandstone that forms the fault-dominated MTD. Location is shown by point 1 in Fig. 1b. Interpretation box in the upper centre of the figure, with sandstone highlighted in yellow in all figures. (b) Pop-up block contained between a thrust and a back thrust. Location and orientation shown in Fig 3a. (c) Thrust fault propagation from an inbricate thrust into the underlying mudstone, yellow and green lines are offset marker beds within the mudstone sequence. Location and orientation shown in Fig 3a. (d) Flame structure between the sandstone layer and the underlying mudstone, suggesting a depositional contact, note the thin, lighter coloured debrite layer a few centimetres below the contact. Location and orientation shown in Fig 3a. (e) Thrust fault producing a brittle offset of the debrite and the mudstone. Note the lateral thickness change of the debrite from thiner (left) to thicker (right). Location and orientation shown in Fig 3a.

Fig 4: (a) Photo (oblique to the inferred transport direction), showing two sandstone blocks embedded within the debrite. Location is shown by point 4 in Fig. 1b and 2a. Interpretation box on the upper centre of the figure highlights sandstone in yellow and debrite in grey. (b) Photo (oblique to the inferred transport direction) showing a sandstone block sitting on top of the mudstone succesion. A

745 thin debrite layer thickens toward the WSW. Note the folding of the sandstone layers on the mudstone
746 succesion. Location is shown by point 3 in Fig. 1b and 2a. (c) Detailed photograph of the irregular
747 contact between the sandstone block and the underlying mudstone succesion. Note the downward
748 sand injections and the proximity of the debrite to the contact. Location is shown in in Fig. 4a. (d)
749 Photo (oblique to the inferred transport direction), showing the relationship between the three units
750 (sandstone, mudstone and the debrite). Location is shown by point 2 in Fig. 1b, 2a and 3a. (e and f)
751 Detailed photographs of the downward pointing sand injections which truncate bedding (white
752 dashed line) in the mudstone sucession Also note the mud clast and seams a couple of centimetres
753 above the contact. Location shown in Fig 4d.
754
755 **Fig 5**: (a) Detailed photograph showing a pinch-and-swell structure on the upper limb of a
756 recumbent fold. Location is shown in Fig. 4b. (b and c) Example of mud clasts and anastomosing mud
757 seams at the sandstone base. Location is shown in Fig. 4a. (d) Example of downwards debritic
758 injection truncating the mudstone succession. (e) Different styles of debritic injections as it intrudes
759 upwards to form diapir-like structures that deform the adjacent mud layers, and lateral spread as sill-
760 like features that also form pinch-and-swell like geometries. Location is shown in Fig. 4d. (f) Debritic
761 infilling necked areas where sandstone layers undergo boudinage. Note the lateral thickness change of
762 the debrite. Location is shown in Fig 3a. (g and h) Examples of ripped-up sandstone and mudstone
763 clasts embbeded in the debrite. Location of g is shown in Fig. 5f.
764 **Fig 6**: Simple sketch showing the organization of the main sedimentary and structural elements
765 of the fault-dominated MTD into block- and imbricate-dominated. (a) Model explaining the
766 generation and formation of the block-dominated MTD. Where sand was fragmented by the flow,
767 pebbly muds were injected upwards into the overlain units, at the same time the sand blocks sunk into
768 the mud. (b) Model showing the generation and deformation of the imbricate-dominated MTD. Where
769 the sand layer was compressed, leading to imbricate thrust slices, the pebbly muds were injected
770 upwards into the overlain units, thus separating the inbricate-dominated from the block-dominated
771 domains. Units legend are the same as Fig. 2.
772

773 **Fig 7**: Photo (looking along the main transport direction), showing the fold-dominated MTD.
774 Pink line marks the top of the unit, overlying yellow line shows a turbidite, and orange marks debritic
775 units. Location is shown by point 5 in Fig. 1b. (b) Top of the deposit showing truncation of the
776 underlying folds of the MTD, and the erosive contact between mud and sandstone beds. Location is
777 shown in Fig. 7a. (c) Example of asymmetrical recumbent folds within the MTD. Location is shown
778 in Fig. 7a. (d) Stereonet showing the distribution of fold hinges as filled circles, SE verging folds
779 (blue circles) and NW verging folds (red circles), Poles to axial planes separated into SE verging folds
780 (blue squares) and NW verging folds (red squares). Mean axial planes intersect and suggest a mean
781 transport direction towards the NE. (e) Doubly-vergent fold contained between two shear planes.
782 Location is shown in Fig. 7a.
783 **Fig 8**: (a) Summary cartoon viewed into the main transport direction, showing the overall fold-
784 dominated MTD. (b) Cartoon showing the 5 end-members of fold hinge evolution, from asymmetric
785 folds (less deformed) to rotated hinges (higly deformed). Examples of each end member are labeled
786 within the outcrop in Fig 7a from 1 to 5. (c) Photo showing two end members of fold hinge shearing
787 evolution, b2: incipient shearing and b4: limbless fold. Location is shown in Fig 7a and 8a. (d) Photo
788 showing an example of b3) sheared fold limb end member. Location is shown in Fig 8a. (e) Example
789 of b5) fold hinge rotation, note the 'Z' folds below the sandstone block. Location is shown in 8a.
790
791 **Fig 9**: (a) Photo of the debritic interval that is rich in elongated mud clasts. Location shown by
792 point 6 in Figure 1b. (b) Rose diagram of mud-clast long axis orientation, showing a mean NE-SW
793 trend. (c) Slump fold showing a cleavage (red lines on the left) axial-planar to slump fold hinges.
794 Location shown by point 7 in Figure 1b. (d) Detailed photograph of the relation between a slump fold
795 and the axial planar cleavage. Location is shown in Fig 9c.
796
797 **Fig 10**: Comparison of the outcrop features and geometries with a layer-normal shearing model.
798 (a) Photo looking along the mean transport direction. (b) Layer-normal shearing model (modified
799 from Alsop and Holdsworth, 2007).
800

801

Figure 1_Location_Map

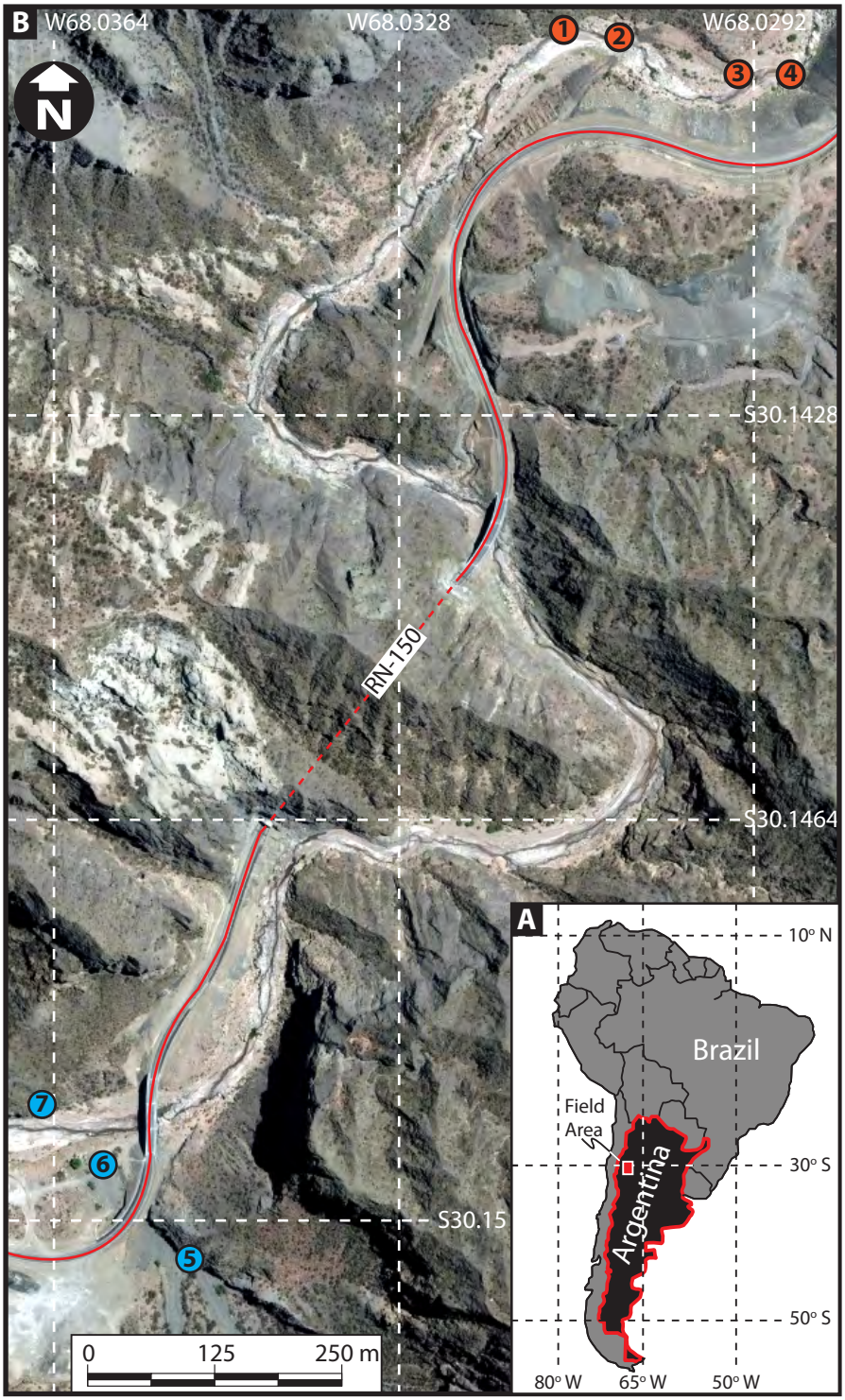

Figure 2_Fault dominated MTD_Schematic_drawing

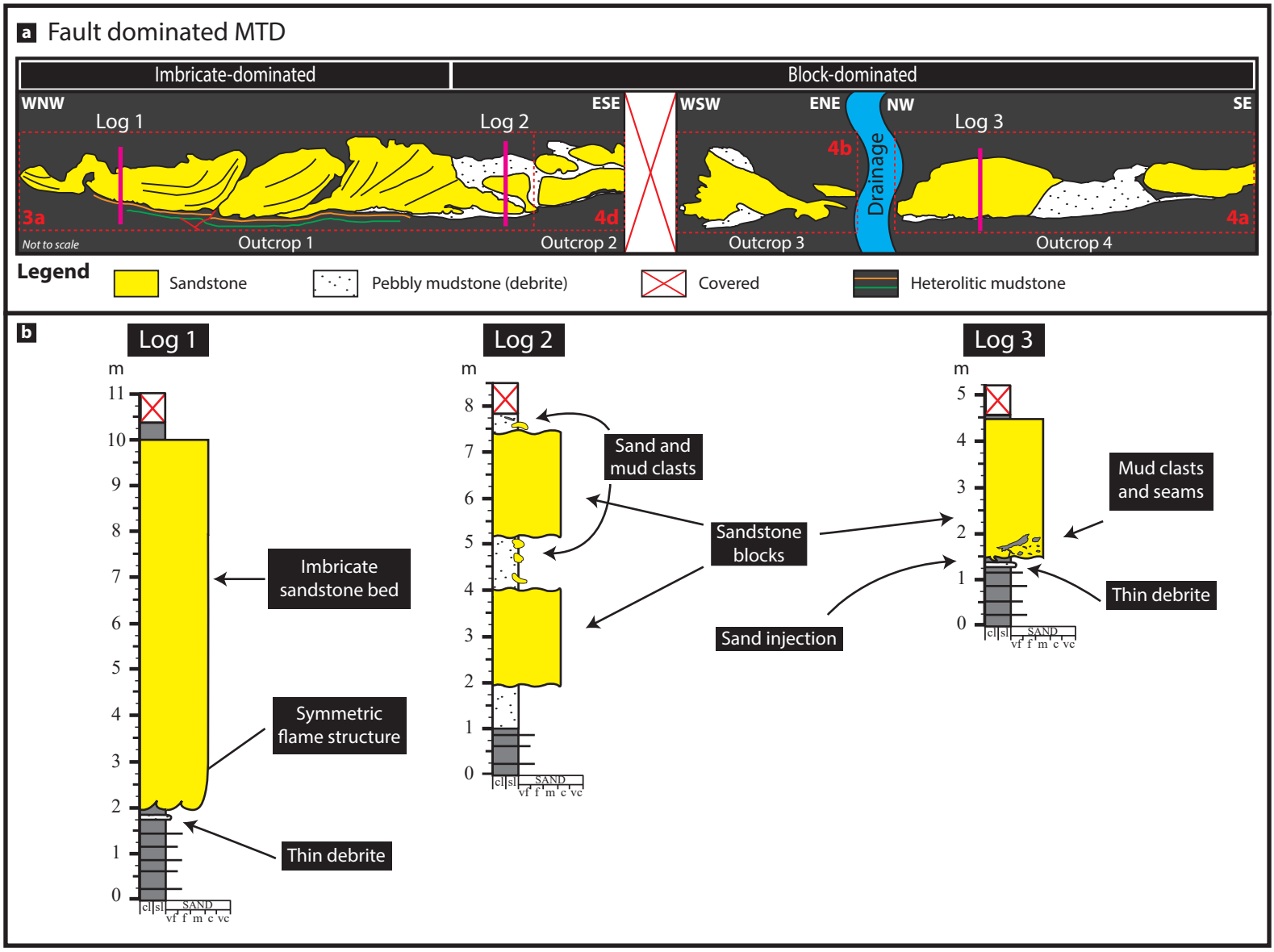

Figure 3. Imbricate dominated

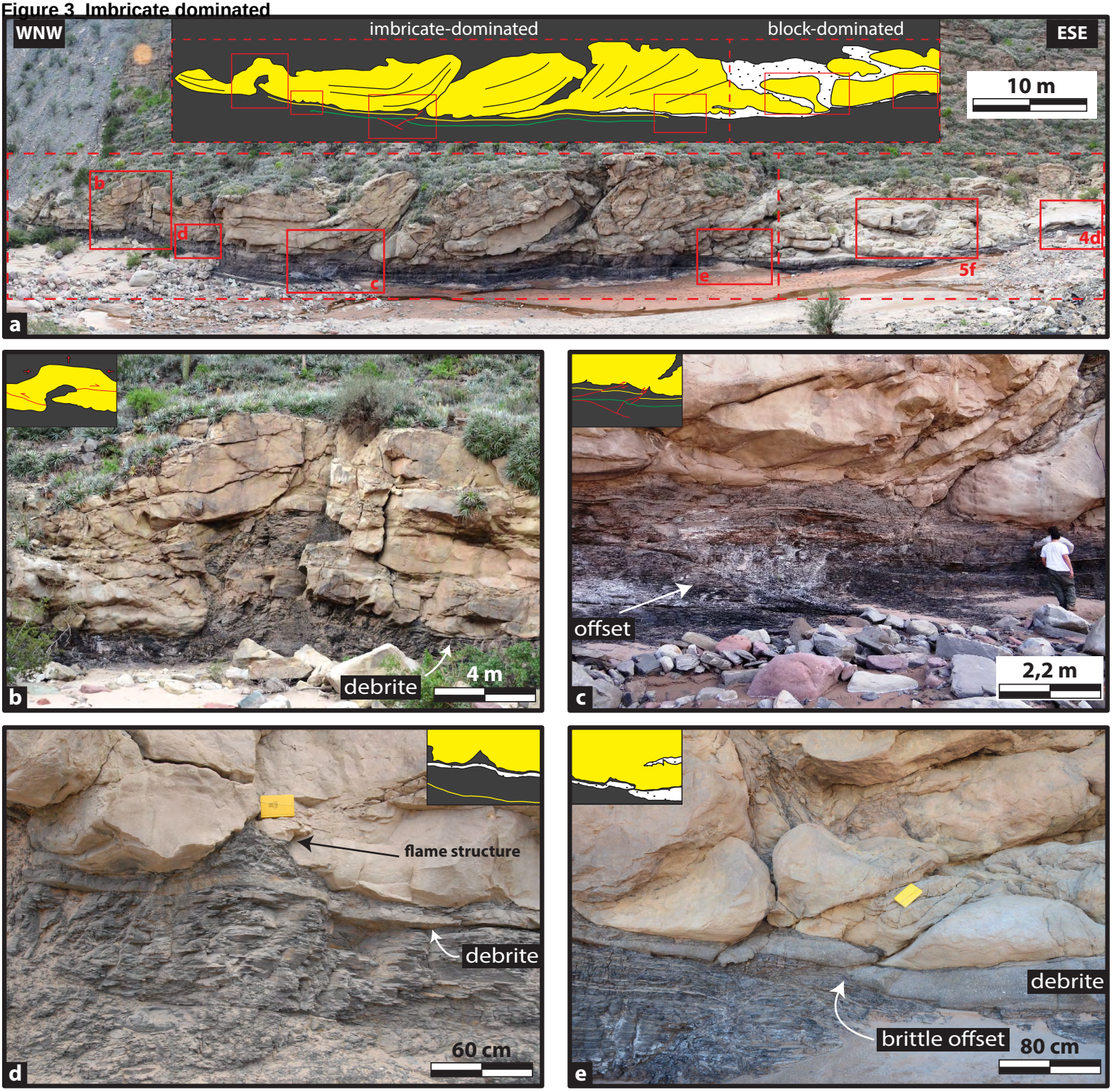

Figure 4. Block dominated

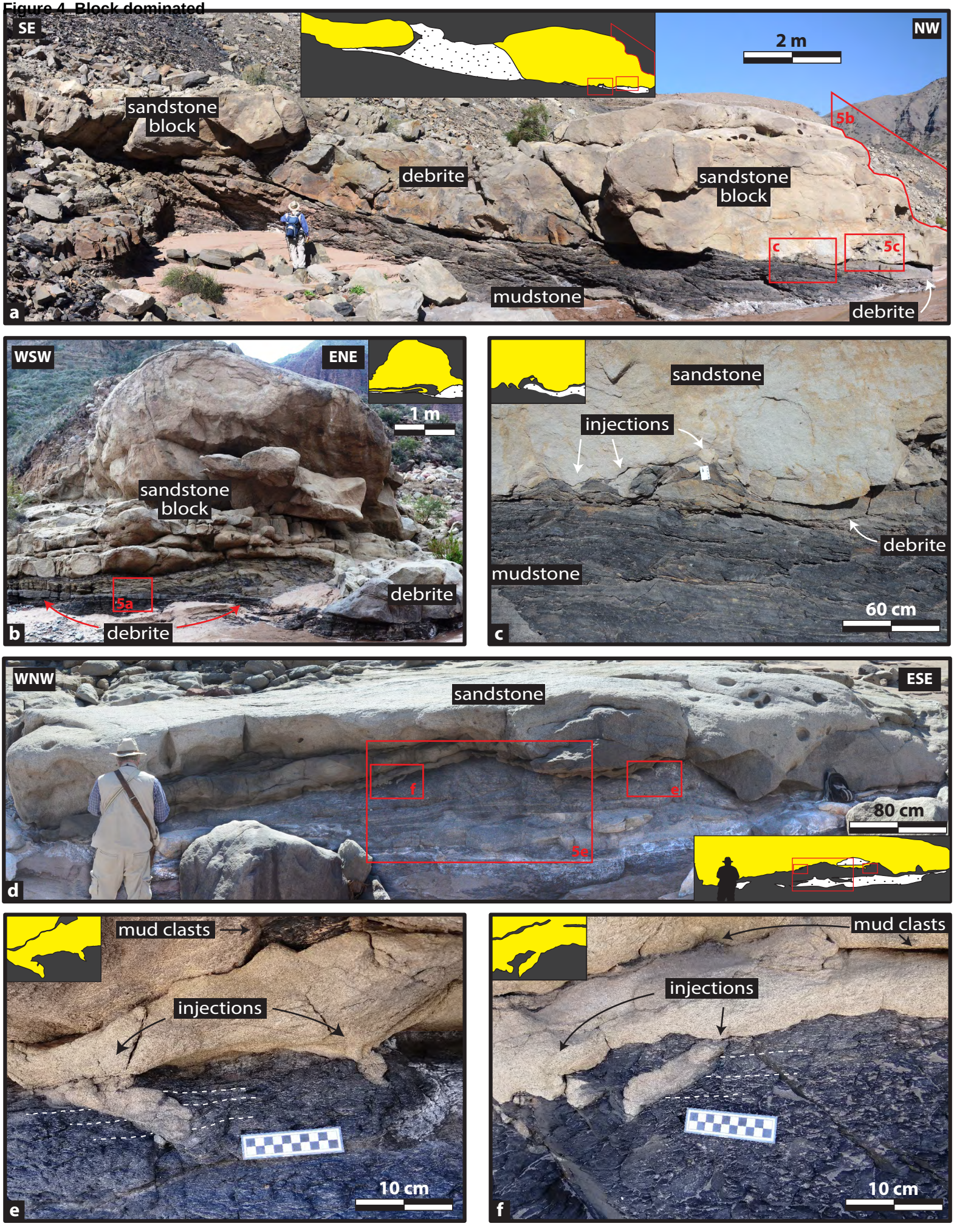

Figure 5_Block dominated

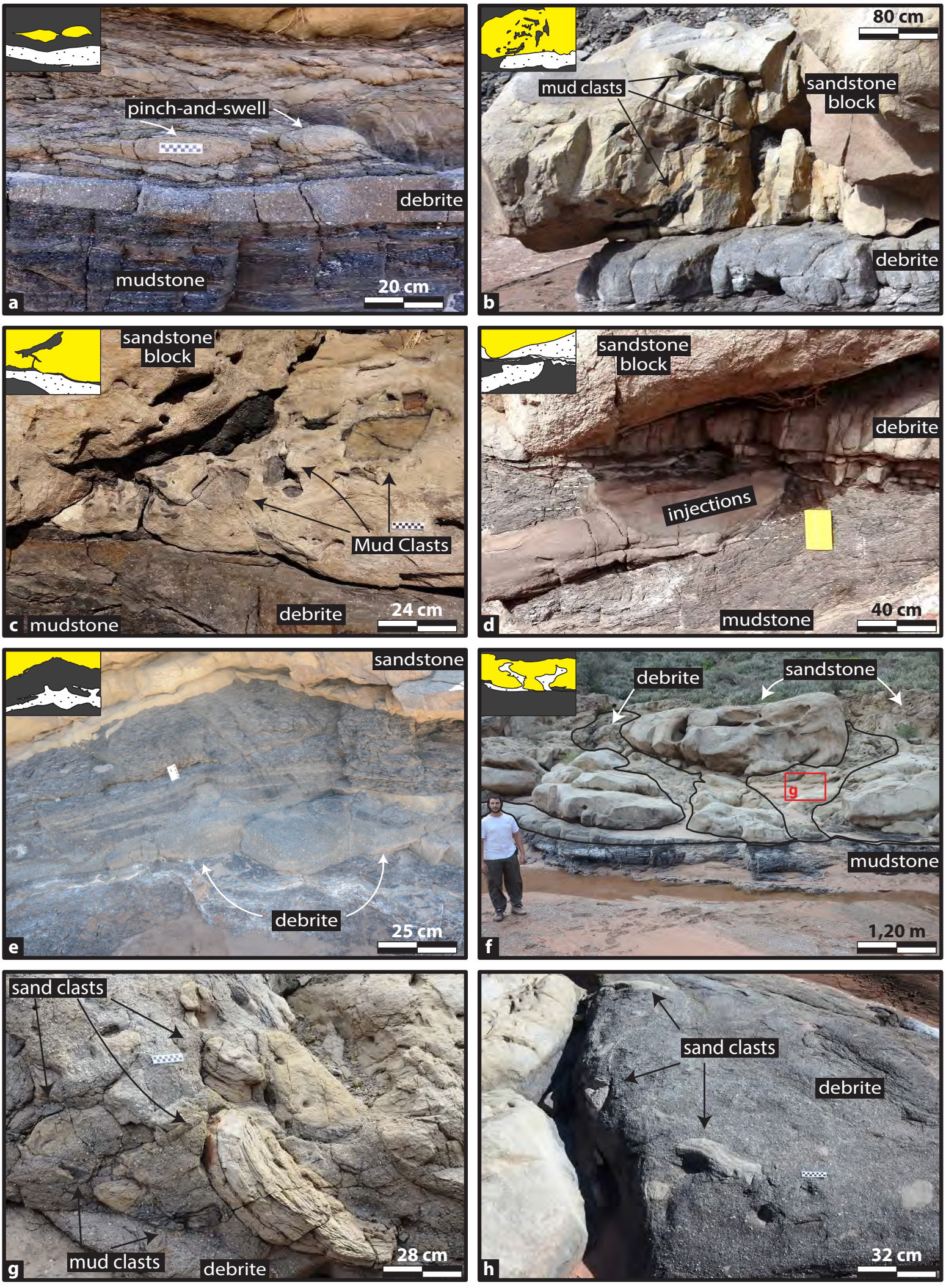

Figure 6_Emplacement_Models

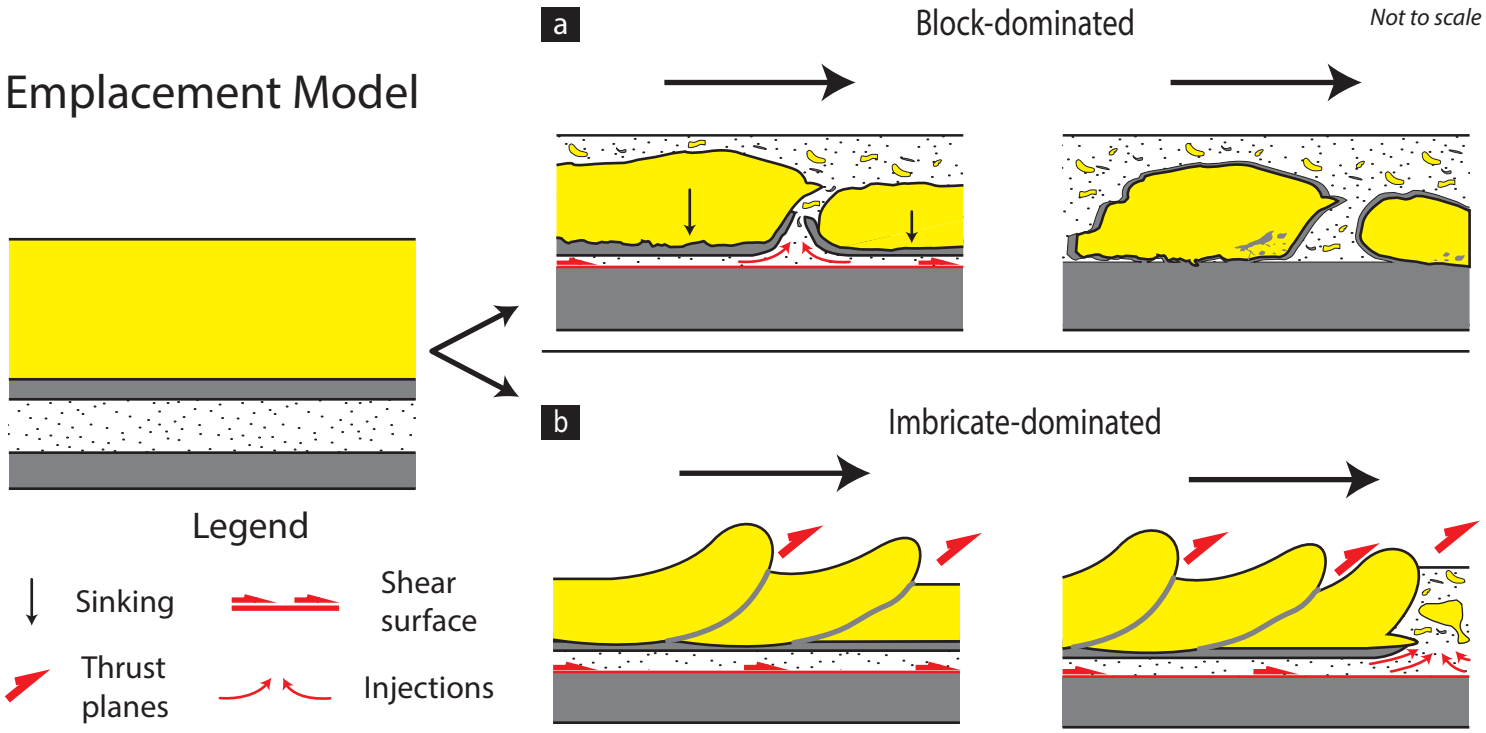

Figure 7_Slump_MTD

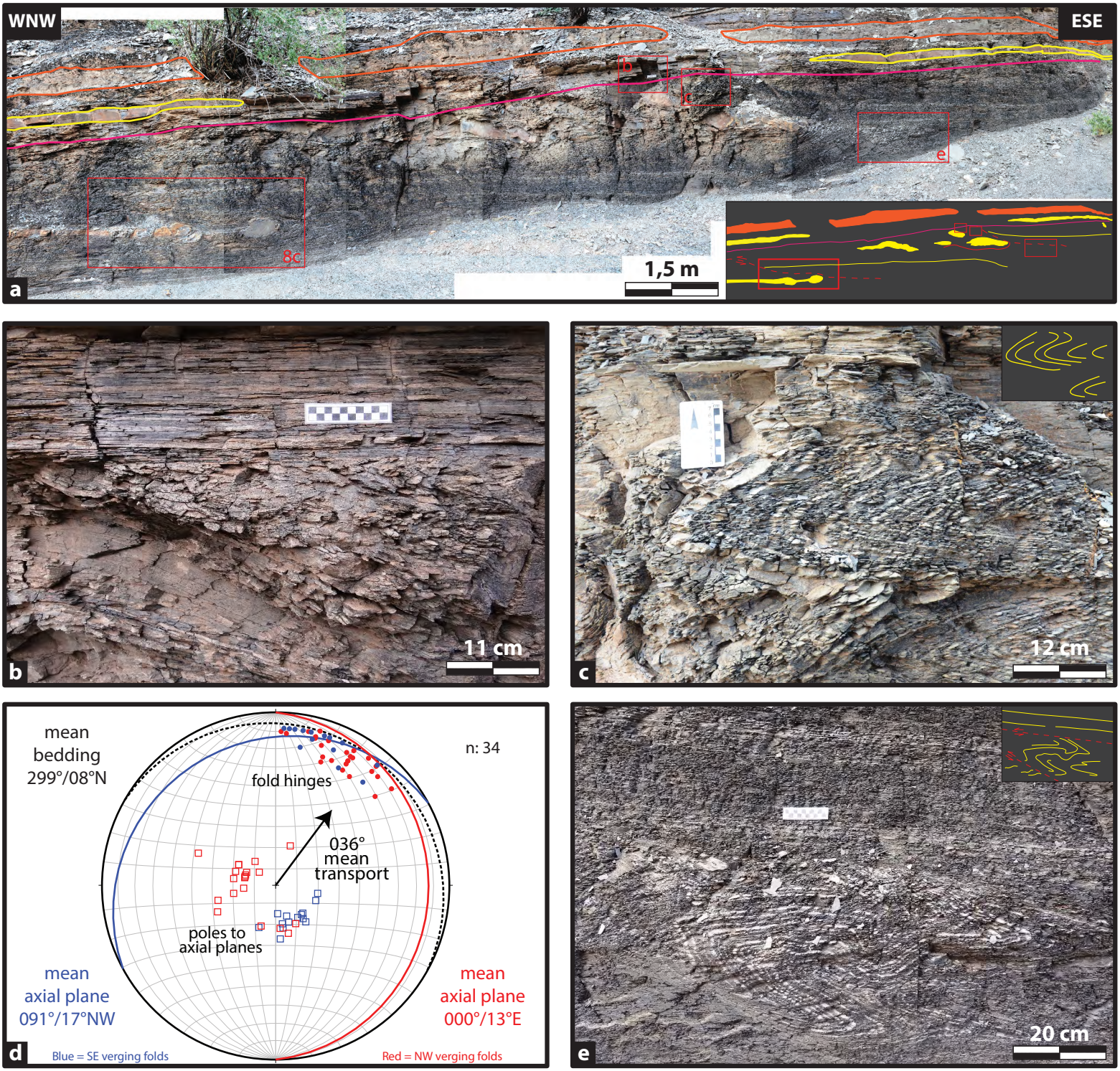

Figure 8_Slump_MTD

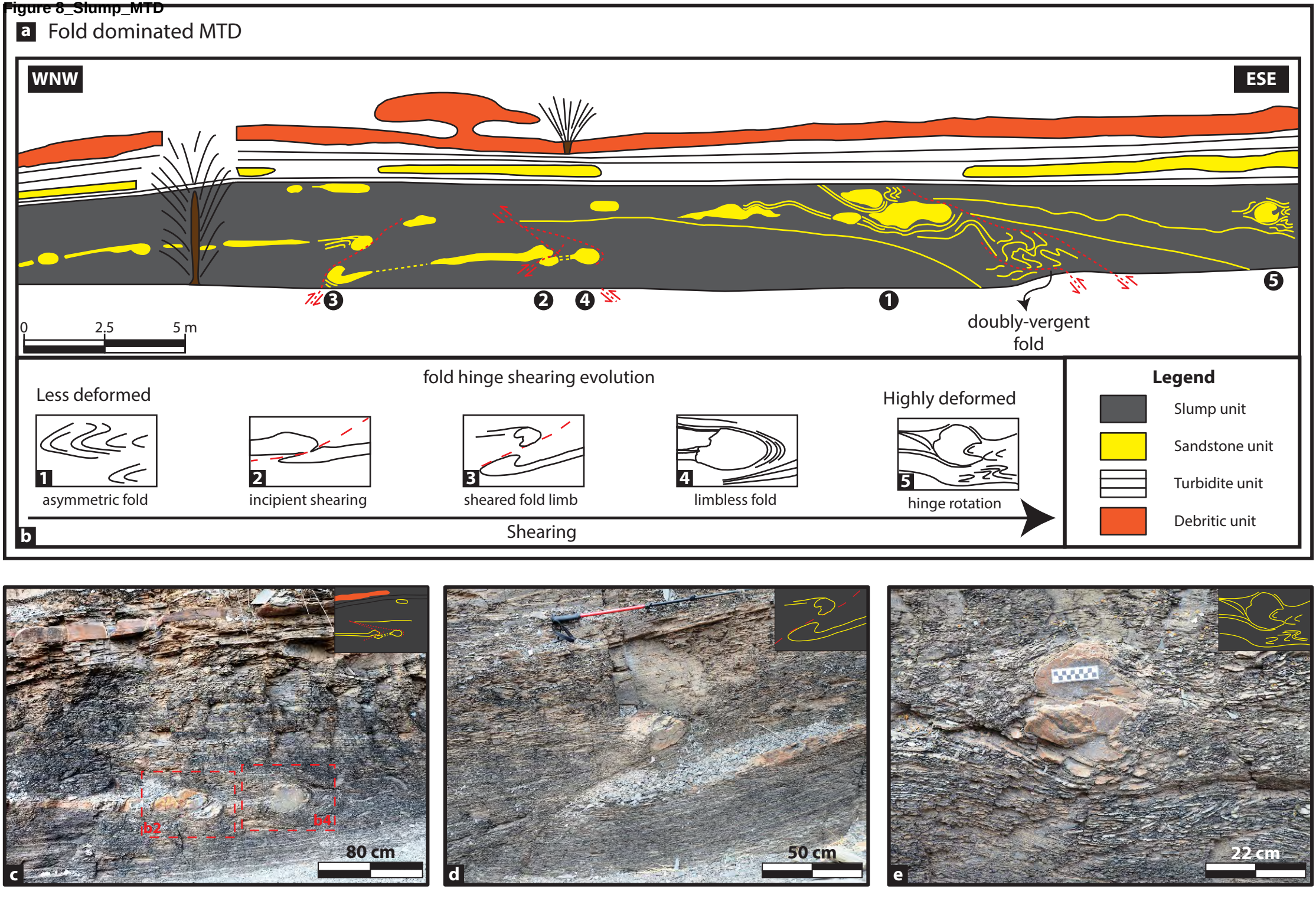

Figure 9 Mud ships

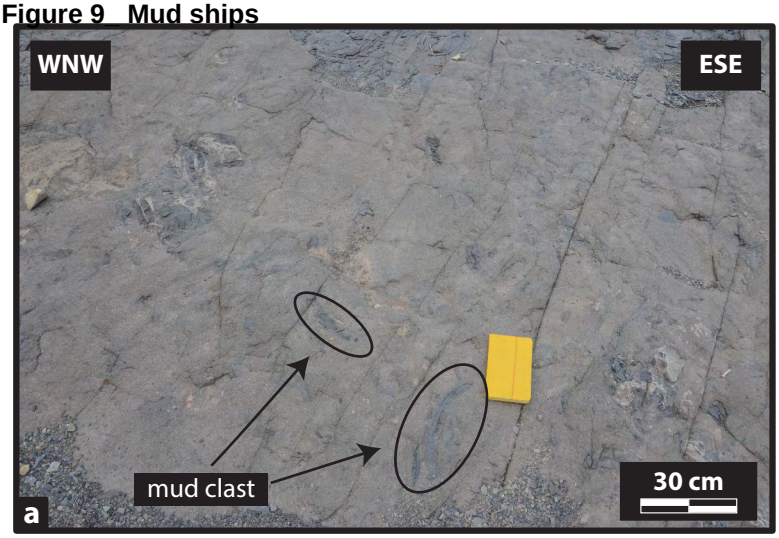

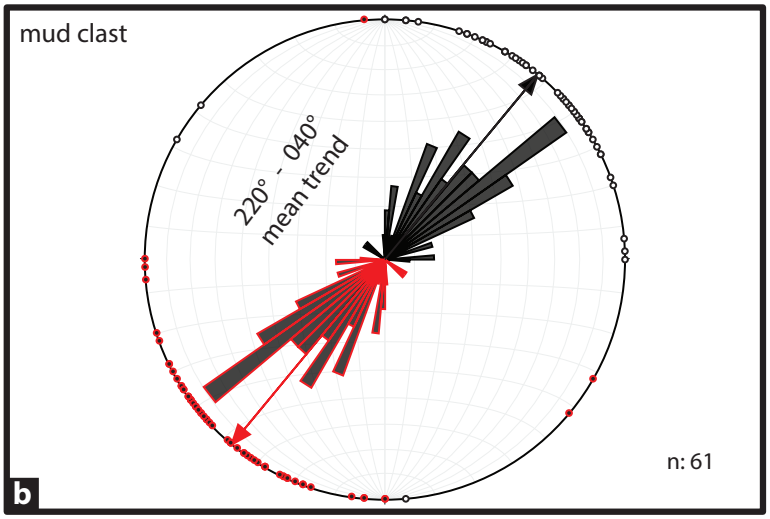

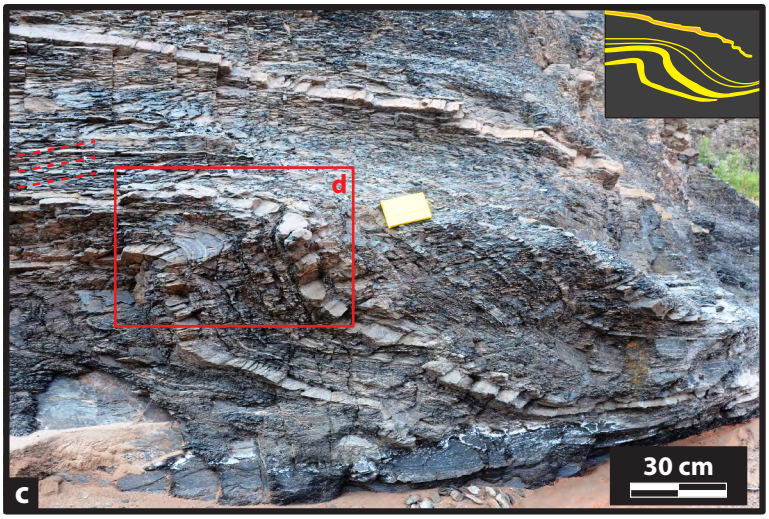

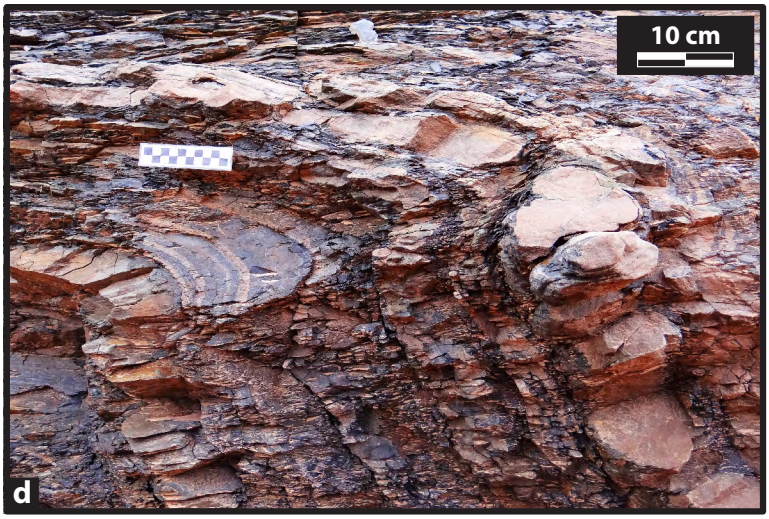

Figure 10_Axial_plane_rotation